IJASRM

International Journal of Advanced Scientific Research and Management, Volume 3 Issue 10, Oct 2018

www.ijasrm.com

ISSN 2455-6378

CFD Analysis of Aerodynamic Interference Effect for a Multibody Launch Vehicle

M.Senthil Kumar[1] and R.Gowrishankar[2]

[1,2]Asstt. Professor, Department of Mechanical Engineering, V.M.K.V Engineering College, Salem, T.N., India

Abstract

Aerodynamics of a multi-body launch vehicle with strap-on is highly dominated by aerodynamic interference effects. The interference effects between core and strap-on varies mainly with gap between the core and the strap-on, strap-on/core diameter and location of the strap-on with respect to the core. The transonic Mach number (M) is selected in this study, since the variation of aerodynamic coefficients including interference effects are high. In general, the vehicle experiences changes in force, moment and drag in the presence of boosters. In this study, the effect of geometric parameters on aerodynamic interference such as strap-on core gap and strap-on diameter are simulated using CFD code at M= 0.9, $\alpha=2^{o}$and Reynolds number of 15 million. The pressure coefficient (C_P), normal force derivative ($C_{N\alpha}$), center of pressure location (X_{cp}) and axial force coefficient (C_A) have been extracted for all configurations. The final result of analysis indicates that strap-on diameter has larger influence on aerodynamic interference effect compared to the strap-on core gap. The interference effect between the core and strap-ons are largest at the highest strap-on diameter.

Keywords— *Interference effect, Multi-body, Core, Strap-on, Transonic, Mach number, Reynolds Number, Pressure coefficient (C_P), Normal force derivative ($C_{N\alpha}$), Center of pressure location (X_{cp}), Axial force coefficient (C_A).*

1. Introduction

This chapter provides an introduction about the Launch vehicle and importance of the present project with respect to launch vehicle aerodynamic interference effect. The aim of this work is explained first followed by the objective of this work. The final section of this chapter outlines the entire thesis, with a summary of the each chapter. Launch vehicles are used for delivering payloads to a specified altitude at specified orbital velocity. In general, the high orbital velocities are difficult to achieve with a single stage vehicle. Therefore, the multistage launch vehicles are used for launching satellites worldwide. Parallel staging of core and strap-on are seen in many launch vehicle and it is one of the most frequently used configurations. In this type of staging, 2 to 9 solid or liquid propellant boosters join the first stage as strap-ons. They are usually ignited simultaneously together with the core engine(s) to provide the maximum thrust, and are separated from the core upon burn-out, to reduce the total weight during ascent trajectory. The strap-on boosters usually have large volumes and affect the external size and shape considerably. The complex flow field around the multiple bodies and the interference effects among them plays a major role in the vehicle's aerodynamics. The vehicles experiences higher or lower force, moment and drag in the presence of boosters and safe separation of the boosters in an interference dominated flow field is also important for the stage separation studies.

2. Literature Review

Ahamed S, Selvarajan S (1991), investigated the flow field on a hammerhead nose configuration at transonic speed. The flow field at transonic Mach number of a hammerhead nose configuration with boat tail angles in the range of 0^{o} to 90^{o} is studied through surface flow visualization and surface pressure measurements. The surface steady pressure data shows presence of a shock on cylindrical portion of the body that shifts downstream with increase in Mach number and boat tail angle. The result of the test shows that variation of the boat tail angle does not induce any additional low frequency unsteadiness in cylindrical region.

Arash Naghib, Amir Nejat, Taravat Khadivi (2002), analyzed Aerodynamic characteristic of launch vehicle with strap-on boosters. An engineering code has been developed for estimation of longitudinal aerodynamic coefficient of multibody

launch vehicle with strap-on boosters, based on their geometric characteristics and flow conditions. The code, which incorporate data from analytical method, CFD analysis, wind tunnel tests and similar engineering code has been used for parametric analysis of the effect of angular position of strap-ons, the gap between the core and strap-ons, angle of attack, the mach no on aerodynamic coefficients (C_N and C_A) of the geometry, defined by statistical investigation of actual launch vehicles. The final result indicated suitable accuracy within range of $0^0<\alpha<16^0$ and M<5.0 for the purpose of preliminary aerodynamic design

Basso E, Azevedo J.L.F (2004), analyzed the three-dimensional viscous flow simulation over the VLS using overset grids. This paper is primarily concerned with presenting results of laminar and turbulent viscous simulations of flows over the first Brazilian satellite launch vehicle, during its first-stage flight. The flight configuration of the VLS is composed by a central body and 4 strap on boosters arranged symmetrically around this central body. The results also highlight interesting features of the flow over the complete VLS and point out the importance of the inclusion of viscous effects for flow simulation over such complex vehicles.

Devasia K.J (1982), investigated of inviscid flow field interference effects in Strapon configurations by panel method. In this, describes the studies on launch vehicle aerodynamics and flow around various geometries of launch vehicle are modeled using panel method to study the effect of geometric parameters such as number of Strap-ons, the ratio of strap-ons radius to sore stage radius an the gap between the core and strap-ons on the vehicle's aerodynamic characteristics

Enda Dimitri, Azevedo F, Leonardo Costa (2007), investigated about turbulent flow simulations of Launch vehicle configurations describes the inviscid flow over the VLS in its first stage and second stage flight configurations are simulated for Transonic (M=0.9) and supersonic (M=2) Mach numbers using adaptive mesh refinement technique. Turbulent viscous flow over the VLS in its second stage flight for transonic and supersonic Mach number including Angle of attack (α=0 and 2). Because of the boundary layer, this shock wave does not reach the body .The region over the end of the boat tail presents very small velocities, but the boundary layer does not separate because of the turbulent characteristics of the flow. In fact laminar simulations of this flow condition indicate boundary layer separation.

Moraes P, Azevedo J, Fernandez F (1990), analyzed the aerodynamics of the VLS during first stage separation. In this study, the forces and moment carried out on 1/40 and 1/15 smooth models of the VLS with four strap-on boosters in high speed wind tunnel. The test programme included simultaneous measurements on the complete vehicle as well on the booster at Mach number 0.5 – 0.9 and angle of attack of 0^o - 6^o to establish basic aerodynamic co-efficient. The result shows influence of Mach number on the booster side force orientation and a small dependence of the magnitude from booster separation angle.

Zhang Lumen, Yu Zechu, Yan Yongjian (1990), reported numerical solution of inviscid supersonic flows around a launch vehicle with four strap-on boosters. The overlapping grid technique has been used to simulates the flow in the gap and local subsonic flow in the region at a non-zero angle of attack have been addressed from the first time in this study. The effect of gap size and Mach number on the interference dominated flow field around the vehicles are investigated. The result showed that all the significant feature of inviscid supersonic over multi-body configurations are captured. The calculation results show good argument with experimental result.

3. Configuration Study

3.1 Brazilian VLS configuration

In the present study, the variants of the baseline configuration are arrived by perturbing gap length and strap-on diameter. The baseline configuration is a multi-body Launch Vehicle known as Vertical Launch System (VLS) of the Brazilian Space Agency.The VLS-1 development started in 1984, after the first launch of the Sonda IV rocket. Till date, three prototypes have been built and two launches attempted, departing from the Alcântara Launch Center. The flight configuration of the first stage of the VLS composed by a central body and four strap-on boosters arranged symmetrically around this central body shown in Fig. 1

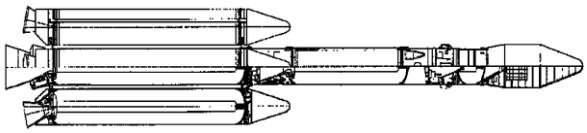

Fig 1. Schematic representation of the VLS

IJASRM

International Journal of Advanced Scientific Research and Management, Volume 3 Issue 10, Oct 2018

www.ijasrm.com

ISSN 2455-6378

3.2 Configurations modeling

The various multi-body launch vehicle configurations are modeled using CATIA V5, a multi-platform CAD/CAM/CAE commercial software suite. This is based on parametric solid modeling design tool used to create fully associative 3D solid models, with or without constraints, while using automatic or user-defined relations to capture the design intent. CATIA graphically displays the feature based structure and other non-graphical data of the model in the form of a specification tree.

Initially, the core was modeled and then the strap-ons were modeled with the axis of the core as reference. The generated launch vehicle (CATIA) model is used to calculate the accurate wetted areas of core and strap-ons. The strap-on attachment, nozzles are not simulated, since the experimental results were also without these components.

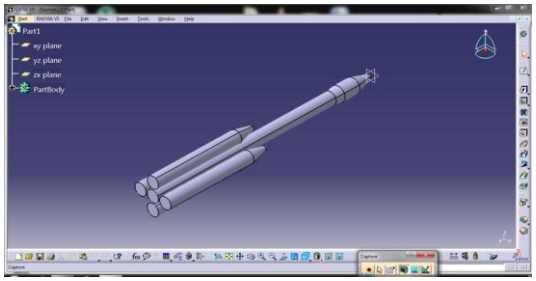

Fig 2. CATIA modeling of nominal VLS configuration

4. Computational Tool

4.1 Computational Fluid Dynamics (CFD)

CFD is the major part of the aerodynamic design process along with wind tunnel testing and engineering methods. Here CFD minimize the dependence of cost and time consuming in wind tunnel testing. This results in accelerating the design process, minimizes preliminary development testing, and help create reliable designs of space launch vehicles and their components. At Present the simulation capability and reliability of this method increases due to availability of advanced models and computer hardware.

4.2 PARAS-3D

PARAS-3D is a Reynolds Averaged Navier – Stokes (RANS) Computational Fluid Dynamic solver (CFD) and it solves the external and internal flow problems. PARAS-3D is an abbreviation of Parallel Aerodynamic Simulator -3 Dimensional. This code based on finite volume formulation and using the Cartesian grid. It uses second order accurate Explicit Riemann solver

4.3 Pre Processor

The pre-processor of the PARAS-3D have inbuilt grid generator. The grid generation around the body is generated by means of a Rectangular Adaptive Mesh (RAM) technique. In RAM technique, mesh adapts to the geometry by splitting the cells near the body and in region of large curvature. There are three types of cells in the Cartesian mesh,

1. Air cells (cells fully outside the body)
2. Body cells (cells fully inside the body)
3. Partial cells (cells partially inside and partially outside).

Cartesian grids are inherently non-body-fitted. It virtually neglects the difficulty of grid generation for complex configurations. Particularly, meshes with millions of cells can be achieved in minutes on advanced powerful workstations. Cartesian grids allow planar surface approximations of the surface. Thus, a wall function approach is used in PARAS-3D to improve the simulation robustness for turbulent simulations.

4.4 Post Processor

PARAS-3D has got inbuilt post processor, where complete analysis of a simulation can be carried out. It can plot 2D line plots, and 3D vector, contour plots. The post processor integrate force and moment coefficiens based on the given reference parameters. The PARAS-3D CFD Solver is given in fig 3

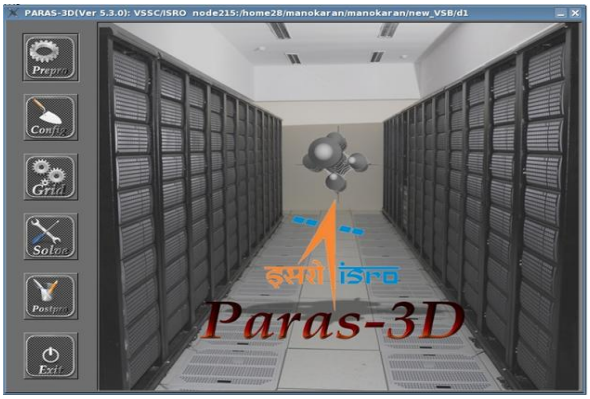

Fig 3. PARAS-3D solver

5. Grids and Simulation Condition

The PARAS-3D pre-processor generate Cartesian grids on the arbitrary of the configurations. The

IJASRM

International Journal of Advanced Scientific Research and Management, Volume 3 Issue 10, Oct 2018

www.ijasrm.com

ISSN 2455-6378

mesh adapts to the geometry by splitting the cells near the body and in region of large curvature. The number of total cells, gas cells, partial cells and body cells for various multi-body configurations are mentioned in the appendix A. The number of initial grids required is based on the complexity of the configuration and that to capture the flow field effectively. The boundary conditions, the domain size, number of initial grids are given in Table 1 The total number of final grid cells captured in the nominal configuration is 33.20 million and the solution is terminated at 180,000 iterations after the convergence. To study the grid independency, the grids were refined at every 30,000 iterations

S. No	Axis	Coordinate Minimum		Coordinate Maximum		Initial Grid Points
		Min. Distance (m)	Boundary Conditions	Max. Distance (m)	Boundary Conditions	
1	X	-40	Upwind	60	Pressure	300
2	Y	-60	Pressure	60	Pressure	300
3	Z	-60	Symmetry	60	Pressure	300

Table 1. Details of Domain, Boundary Conditions and Grids

Wall boundary condition is applied on the configuration solid surface. It can be noticed from the figure, that near the solid body boundaries, the grids are refined such that it captures the body shape for the given body capture/grid refinement criteria. The computational parameters setting in the PARAS-3D solver shown in fig 4

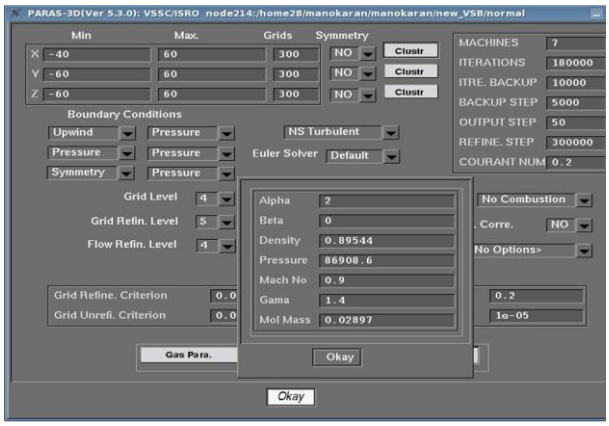

Fig 4. Computational settings in PARAS-3D solver

6. Results and Discussion

CFD simulations were first carried out for the nominal configuration using PARAS-3D solver with k-ε turbulence model at Mach number 0.9, angle of attack 0° and Reynolds number 15 million. The results were compared with the available experimental results for validation. The simulations were then carried out on the MBLV configurations for various gap lengths and diameter of the strap-ons at Mach number 0.9, angle of attack 2°and Reynolds number 15 million. In this flight condition, strong shock wave builds over the cylindrical portion of the heat shield region and the strap-ons, whereas other flow regions are transonic. The pressure coefficient (C_P), normal force coefficient ($C_{N\alpha}$), center of pressure location (X_{cp}) and axial force coefficient (C_A) were extracted for all configurations and compared with nominal configuration.

6.1 Variation of C_P for Nominal configuration at α=2°

The pressure and mach contours for the nominal configuration at Mach number 0.9, angle of attack 2° and Reynolds number 15 million. The regions of stagnation and supersonic expansion were observed. The flow expansion is higher in the interference region at the windward side. Supersonic pockets are also seen at the leeward side of the nose cap corner of the strap-on and at the interference regions.

6.2 Variation of C_P for Gap variants at α=2°

It shows the variation of C_P of the MBLV configuration for the gap variants over the leeward, windward and side of the core body. It was observed that the variation of C_P is negligible for the gap variants

6.3 Variation of C_P for Diameter variants at α=2°:

It shows the variation of C_P with the diameter variants on the leeward, windward and side of the core. It was observed that C_P varies with the variation in diameter of the strap-ons. It was observed that the strap-on with the highest diameter showed the largest value of C_P at the stagnation point in front of the nose cap and lowest C_P at supersonic expansion. The increase in diameter of the strap-on increases the nose cone angle of the strap-on. The expansion at the nose cap corner of the strap-on is the same for all diameter variants. The value of$C_P$shows the highest peak at the largest strap-on diameter after the expansion at the nose corner due to the increased cone angle. This increased cone angle creates a shift in the curve due to delay in expansion and higher expansion at the cone cylinder intersection with the increase in strap-on diameter. The supersonic expansion is

IJASRM

International Journal of Advanced Scientific Research and Management, Volume 3 Issue 10, Oct 2018

www.ijasrm.com

ISSN 2455-6378

followed by a shock across which the flow gradients vary.

6.4 $C_{N\alpha}$ variation with Gap and Diameter variants

In the present study a nominal gap of 0.1 m exists between core and the strap-on. The size of this gap affects the aerodynamic interference effect between core and the strap-on. The figure indicates that an increase in gap shows a linear decrease in $C_{N\alpha}$. As the gap between the core and the strap-on is decreased the flow accelerates in the interference region. The boundary layers of strap-on and the core are disturbances to the flow creating a narrow flow path. This low pressure created at the interference region acts on the walls of the strap-on and core, thus increasing the $C_{N\alpha}$. The increased gap reduces the flow acceleration creating a constant pressure, thus reducing the $C_{N\alpha}$.

From the figure 5 it can be noticed that $C_{N\alpha}$ increases quadratically with the increase in strap-on diameter. $C_{N\alpha}$ increases with the area exposed to the flow. Thus, the strap-on with the highest diameter showed the largest value of $C_{N\alpha}$ compared to the nominal configuration. The decrease in $C_{N\alpha}$ was 8% between the lowest and highest gap lengths and showed an increase of 83% between the lowest and highest strap-on diameter with reference to the nominal diameter.

The $C_{N\alpha}$ increase in the highest strap-on diameter was 36% when compared with the nominal configuration, 24% increase in $C_{N\alpha}$ for 20% increase in strap-on diameter, 25% decrease in $C_{N\alpha}$ for 20% reduction in strap-on diameter

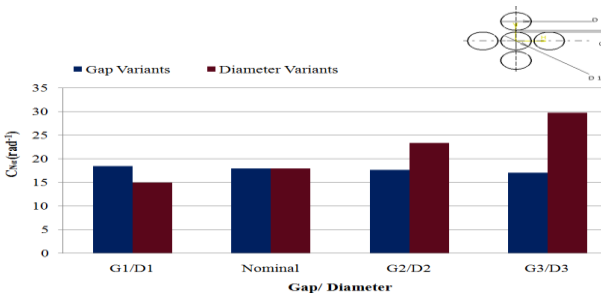

Fig 5. Comparison of CNα for diameter and gap variants with the Nominal configuration

6.5 X_{cp} variation with Gap and Diameter variants

Fig 6 shows the variation of Xcp with gap and diameter variants. It was observed that Xcp increases with the increase in gap length and increase in strap-on diameter. Xcp shows an increase of 8.7% between the lowest and highest gap lengths and an increase of 20% between the lowest and highest strap-on diameter with reference to the nominal diameter. The strap-on with the highest diameter indicates the location of the normal force at a larger distance from the reference axis.

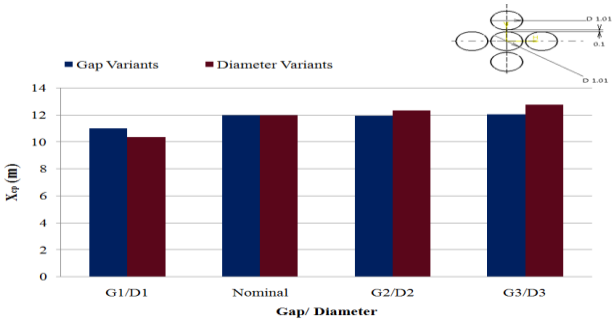

Fig 6. Comparison of Xcp for diameter and gap variants with the Nominal configuration

6.6 C_A variation with Gap and Diameter variants

It shows the cumulative C_A plot for the MBLV for gap and diameter variants. It was observed that the cumulative C_A showed the highest value for the largest strap-on diameter and the lowest gap length between the core and strap-on.

Fig 7 shows the C_A plot for the gap and diameter variants. It was observed that the variation in C_A was negligible for the gap variants. The value of C_A decreases with the increase in gap length between the core and the strap-on. It shows a decrease of 3% between the lowest and highest gap lengths with reference to the nominal diameter. The value of C_A increases with the increase in strap-on diameter. It shows an increase of 157% between the lowest and highest strap-on diameter with reference to the nominal diameter

The axial force coefficient was calculated considering the pressure drag alone. Skin friction drag was not considered assuming the surface to be a smooth surface.

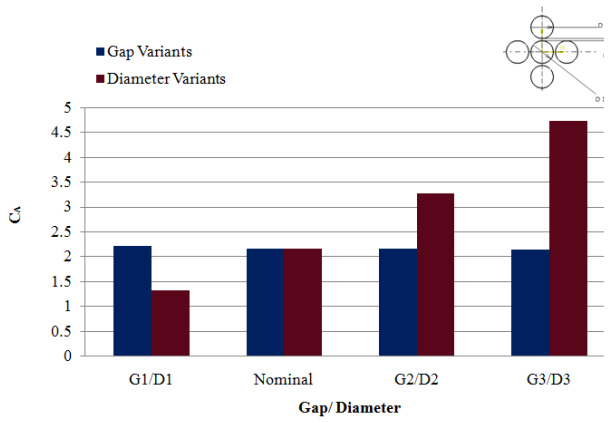

Fig 7 Comparison of CA for diameter and gap variants with the Nominal configuration

7. Conclusion

In this the aerodynamic analysis of the Multi-Body Launch Vehicle at different geometric parameter is studied for interference ef the PARAS-3D software at 2^0 angle of attack in the transonic Mach number 0.9. The normal force coefficient (CNα), pressure force coefficient (Cp), centre of pressure location (Xcp) and axial force coefficients (CA) have been extracted for all geometric conditions and compared with the nominal configuration.

Cp shows negligible variation for the various gap lengths. CNα decreases as the gap length is increased, Xcp and CA increases wi strap-on diameter. The increase in CNα was 83%, Xcp shows an increase of 20% and CA shows an increase of 157% between the lowest and highest strap-on diameter with reference to the nominal diameter.

This indicates that strap-on diameter have larger influence on aerodynamic interference effect compared to strap-on core gap length. The interference effect between the core and strap-on are largest at highest strap-on diameter.

References

[1] Ahmed, S. and Selvarajan, S, 'Investigation of Flow Field on a Hammerhead Nose Configuration at Transonic Speeds', AIAA 22nd Fluid Dynamics, Plasma Dynamics & lasers Conference, AIAA-97-1711, (1991).

[2] Arash Naghib, Amir Nejat, Taravat Khadivi,'Parametric Analysis of Aerodynamic Characteristics of Launch Vehicle with Strap-on Boosters', ICAS- Congress, (2002).

[3] Basso E and Azevedo J.L.F., 'Three dimensional viscous flow simulation over the VLS using overset grids', Journal of the Brazilian Society of Mechanical Science & Engineering, Vol.XXVI, No.4, pp.438-445, (2004).

[4] Devasia, K.G., 'Investigation of inviscid flow field interference effects in strap-on configurations using panel method', 13th Int. Symposium on Space Science and Technology, Tokyo, Japan , (1982).

[5] Enda Dimitri, Azevedo F and Leonardo Costa, 'Centered Upwind Multigrid Turbulent Flow Simulation of Launch Vehicle Configuration', Journal of Spacecraft and Rocket, DOI-10.2514/1.23843, Vol.44, No.1, pp.52-65, (2007).

[6] Moraes P, Azevedo J and Fernandez F 'Aerodynamics of the Brazilian Satellite Launch Vehicle (VLS) during First Stage Separation', AIAA Paper, AIAA-90-3098-CP, (1990).

[7] Zhang Lumen, Yu Zechu and Yan Yongjian 'Numerical Simulation of Inviscid Supersonic Flow over Multiple Bodies', 27th AIAA Aerospace Sciences Meeting & Exhibit, AIAA-90-3099-CP, (1990).